

The Peculiar Transient AT2018cow: A Possible Origin of A Type Ibn/IIn Supernova

DANFENG XIANG,¹ XIAOFENG WANG,^{1,2,3,*} WEILI LIN,¹ JUN MO,¹ HAN LIN,¹ JAMISON BURKE,^{4,5}
DAICHI HIRAMATSU,^{4,5} GRIFFIN HOSSEINZADEH,⁶ D. ANDREW HOWELL,^{4,5} CURTIS MCCULLY,^{4,5} STEFAN VALENTI,⁷
JÓZSEF VINKÓ,^{8,9,10,11} J. CRAIG WHEELER,¹¹ SHUHRAT A. EHGAMBERDIEV,¹² DAVRON MIRZAQULOV,¹²
ATTILA BÓDI,^{8,13,9} ZSÓFIA BOGNÁR,^{8,13,9} BORBÁLA CSEH,⁸ OTTÓ HANYECZ,⁸ BERNADETT IGNÁCZ,⁸ CSILLA KALUP,⁸
RÉKA KÖNYVES-TÓTH,⁸ LEVENTE KRISKOVICS,^{8,14} ANDRÁS ORDASI,⁸ ANDRÁS PÁL,^{8,14,15} KRISZTIÁN SÁRNECZKY,⁸
BÁLINT SELI,⁸ RÓBERT SZAKÁTS,⁸ T. ARRANZ-HERAS,^{16,17} R. BENAVIDES-PALENCIA,^{16,18} D. CEJUDO-MARTÍNEZ,^{16,19}
P. DE LA FUENTE-FERNÁNDEZ,^{16,20} A. ESCARTÍN-PÉREZ,^{16,21} F. GARCÍA-DE LA CUESTA,^{16,22}
J.L. GONZÁLEZ-CARBALLO,^{16,23} R. GONZÁLEZ-FARFÁN,^{16,24} F. LIMÓN-MARTÍNEZ,^{16,25} A. MANTERO,^{16,26}
R. NAVES-NOGUÉS,^{16,27} M. MORALES-AIMAR,^{16,28} V. R. RUÍZ-RUÍZ,^{16,29} F.C. SOLDÁN-ALFARO,^{16,30}
J. VALERO-PÉREZ,^{16,31} F. VIOLAT-BORDONAU,^{16,32} TIANMENG ZHANG,^{33,34} JUIA ZHANG,^{35,36,37} XUE LI,¹
ZHIHAO CHEN,¹ HANNA SAI,¹ AND WENXIONG LI¹

¹*Physics Department and Tsinghua Center for Astrophysics (THCA), Tsinghua University, Beijing, 100084, China*

²*Beijing Planetarium, Beijing Academy of Sciences and Technology, Beijing, 100044, China*

³*Purple Mountain Observatory, Chinese Academy of Sciences, Nanjing, 210023, China*

⁴*Las Cumbres Observatory, 6740 Cortona Drive, Suite 102, Goleta, CA 93117-5575, USA*

⁵*Department of Physics, University of California, Santa Barbara, CA 93106-9530, USA*

⁶*Center for Astrophysics | Harvard & Smithsonian, 60 Garden Street, Cambridge, MA 02138-1516, USA*

⁷*Department of Physics and Astronomy, University of California, 1 Shields Avenue, Davis, CA 95616-5270, USA*

⁸*Konkoly Observatory, Research Centre for Astronomy and Earth Sciences, Konkoly-Thege M. út 15-17, Budapest 1121, Hungary*

⁹*ELTE Eötvös Loránd University, Institute of Physics, Pázmány Péter sétány 1/A, Budapest, 1117, Hungary*

¹⁰*Department of Optics & Quantum Electronics, University of Szeged, Dóm tér 9, Szeged, 6720 Hungary*

¹¹*Department of Astronomy, University of Texas at Austin, Austin, TX, 78712, USA*

¹²*Ulugh Beg Astronomical Institute, Uzbekistan Academy of Sciences, Uzbekistan, Tashkent, 100052, Uzbekistan*

¹³*CSFK Lendület Near-Field Cosmology Research Group*

¹⁴*Eötvös Loránd University, Institute of Physics, Pázmány Péter sétány 1/A, Budapest, 1117, Hungary*

¹⁵*Eötvös Loránd University, Department of Astronomy, Pázmány Péter sétány 1/A, Budapest, 1117, Hungary*

¹⁶*Observadores de Supernovas Group (ObSN), Spain*

¹⁷*Obs. Las Pequeras, 40470 Navas de Oro, Segovia, Spain*

¹⁸*Obs. Posadas MPC J53, 14730 Posadas, Córdoba, Spain*

¹⁹*Obs. El Gallinero, 28192 El Berrueco, Madrid, Spain*

²⁰*Obs. Llanes, 33784 Llanes, Asturias, Spain*

²¹*Obs. Belako, 48100 Mungia, Vizcaya, Spain*

²²*Obs. La Vara MPC J38, 33784 Muñas de Arriba, Asturias, Spain*

²³*Obs. Cerro del Viento MPC I84, 06010 Badajoz, Spain*

²⁴*Obs. Uraniborg MPC Z55, 41400 Écija, Sevilla, Spain*

²⁵*Obs. Mazariegos MPC I99, 34170 Mazariegos, Palencia, Spain*

²⁶*Obs. Bernezzo MPC C77, 12010 Bernezzo, Cuneo, Italy*

²⁷*Obs. Montcabrer MPC 213, 08348 Cabriels, Barcelona, Spain*

²⁸*Obs. Sencelles MPC K14, 07140 Sencelles, Islas Baleares, Spain*

²⁹*New Mexico Skies (USA), iTelescope Siding Spring (Asutralia), AstroCamp (Nerpio, Spain)*

³⁰*Obs. Amanecer de Arrakis MPC Z74, 41500 Alcalá de Guadaira, Sevilla, Spain*

³¹*Obs. Ponferrada MPC Z70, 24411 Ponferrada, León, Spain*

³²*Obs. Norba Caesarina MPC Z71, 10195 Cáceres, Spain*

³³*Key Laboratory of Optical Astronomy, National Astronomical Observatories, Chinese Academy of Sciences, 10101, Beijing*

³⁴*School of Astronomy and Space Science, University of Chinese Academy of Sciences, 101408, Beijing*

³⁵*Yunnan Observatories, Chinese Academy of Sciences, Kunming 650216, China*

³⁶*Key Laboratory for the Structure and Evolution of Celestial Objects, Chinese Academy of Sciences, Kunming 650216, China*

³⁷*Center for Astronomical Mega-Science, Chinese Academy of Sciences, 20A Datun Road, Chaoyang District, Beijing, 100012, China*

(Received October 21, 2021; Revised October 21, 2021; Accepted xx xx, xxxx)

ABSTRACT

We present our photometric and spectroscopic observations on the peculiar transient AT2018cow. The multi-band photometry covers from peak to ~ 70 days and the spectroscopy ranges from 5 to ~ 50 days. The rapid rise ($t_r \lesssim 2.9$ days), high luminosity ($M_{V,\text{peak}} \sim -20.8$ mag) and fast decline after peak make AT2018cow stand out of any other optical transients. While we find that its light curves show high resemblance to those of type Ibn supernovae. Moreover, the spectral energy distribution remains high temperature of $\sim 14,000$ K after ~ 15 days since discovery. The spectra are featureless in the first 10 days, while some broad emission lines due to H, He, C and O emerge later, with velocity declining from $\sim 14,000$ km s $^{-1}$ to ~ 3000 km s $^{-1}$ at the end of our observations. Narrow and weak He I emission lines emerge in the spectra at $t > 20$ days since discovery. These emission lines are reminiscent of the features seen in interacting supernovae like type Ibn and IIn subclasses. We fit the bolometric light curves with a model of circumstellar interaction (CSI) and radioactive decay (RD) of ^{56}Ni and find a good fit with ejecta mass $M_{\text{ej}} \sim 3.16 M_{\odot}$, circumstellar material mass $M_{\text{CSM}} \sim 0.04 M_{\odot}$, and ejected ^{56}Ni mass $M_{^{56}\text{Ni}} \sim 0.23 M_{\odot}$. The CSM shell might be formed in an eruptive mass ejection of the progenitor star. Furthermore, host environment of AT2018cow implies connection of AT2018cow with massive stars. Combining observational properties and the light curve fitting results, we conclude that AT2018cow might be a peculiar interacting supernova originated from a massive star.

Keywords: CSM interaction – supernova: general – : supernova: individual (AT2018cow, SN2006jc)

1. INTRODUCTION

The studies of time domain astronomy cover a variety of optical transients, including novae, supernovae (SNe), tidal disruption events (TDE), and kilonovae, etc. With different physical origins, these transients exhibit a huge diversity in evolutionary properties, especially optical light curves. The evolutionary time scales and luminosity of different transients are directly related to their physical origins. There are a group of transients with very high luminosity and short timescale of evolution, such as the so-called fast evolving luminous transients (FELTs) (e.g. Rest et al. 2018). They have much faster rise and decline in light curves than regular SNe. And many of them have peak luminosity much higher than normal SNe, close to the superluminous supernovae (SLSNe, Quimby et al. 2011; Howell 2017). The physical origins of these FELTs are still unclear. Among them, some are characterized by very blue color, indicating high temperature, which are also called fast-rising blue optical transients (FBOTs, e.g. Drout et al. 2014; Arcavi et al. 2016).

A recently discovered extragalactic transient, AT2018cow (ATLAS18qqn), has caught much attention due to its peculiar behaviour in its light curves and spectral evolution. AT2018cow was discovered by ATLAS on MJD 58285.44 (UT Jun. 16.44, 2018, UT dates are used throughout this paper), with a magnitude of 14.76 ± 0.10 mag in ATLAS *orange*-band (Smartt et al. 2018). It is located far from the center of the host

galaxy CGCG 137-068 ($z = 0.0141$, $D_L = 63$ Mpc 1). This distance means that AT2018cow is as luminous as the peak of SNe Ia at discovery. As soon as this transient source was reported, astronomers from all over the world were actively conducting its follow-up observations in all bands, including ultra-violet (UV), optical, X-ray, radio and γ -ray. AT2018cow is found to evolve rapidly with a rise time less than 3 days and peak magnitude < -20 mag. The photospheric temperature is measured to be $\sim 30,000$ K near the peak and it still maintains high temperature of $\sim 15,000$ K after ~ 20 days after discovery (Prentice et al. 2018; Perley et al. 2019). All of these features suggest that AT2018cow can be put into the FBOTs.

The close distance makes AT2018cow the first FELT/FBOT which has well-sequenced photometric and spectroscopic observations in wavebands ranging from X-ray to radio (e.g., Prentice et al. 2018; Perley et al. 2019; Kuin et al. 2019; Margutti et al. 2019; Ho et al. 2019), making it a rare sample for the study of FBOT-like objects. In previous studies, several possible physical mechanisms have been proposed for AT2018cow, e.g., tidal disruption of a star into an intermediate mass black hole (Perley et al. 2019; Kuin et al. 2019, Li et al. in prep.), central-engine powered supernova (Prentice et al. 2018; Margutti et al. 2019), interaction of a condensed CSM and the supernova shock (Margutti et al. 2019; Leung et al. 2020), electron-capture collapse of a white dwarf (Lyutikov & Toonen 2019). And Margutti et al. (2019) suggests that

* E-mail: wang_xf@mail.tsinghua.edu.cn

¹ We assume a flat universe with $H_0 = 67.7$ km s $^{-1}$ Mpc $^{-1}$, $\Omega_M = 0.307$ (Planck Collaboration et al. 2016).

there should be a deeply embedded X-ray source in an asymmetrical ejecta.

In this paper, we present our optical photometric and spectroscopic observations of AT2018cow. Spectroscopic observations spanned from Jun. 21, 2018 to Aug. 14, 2018. and photometric observations lasted until September 21, 2018. In Sec. 2 we describe our spectroscopic and photometric observations as well as data processing. In Sec. 3 we analyse the observational properties of AT2018cow, including light-curve and spectral evolution. The analysis of the host galaxy is presented in Sec. 4. In Sec. 5 we explore the possible physical origins of AT2018cow. Further discussion and final summary are given in Sec. 6 and 7, respectively.

2. OBSERVATIONS AND DATA REDUCTION

2.1. Photometric Observations

The optical photometric observations of AT2018cow were monitored by several observatories, including the 0.8-m Tsinghua University-NAOC telescope (TNT, Huang et al. 2012) at Xinglong Observatory of NAOC, the AZT-22 1.5-m telescope (hereafter AZT) at Maidanak Astronomical Observatory (Ehgamberdiev 2018), telescopes of the Las Cumbres Observatory network (LCO), and telescope of Konkoly Observatory in Hungary (hereafter KT). Photometric and spectroscopic data from LCO were obtained via the Global Supernova Project (GSP). We also collected early time photometric data from Observadores de Supernovas Group (ObsN) in Spain. The TNT and LCO observations were obtained in standard Johnson-Cousin *UBV* bands and SDSS *gri* bands. Long time and short-cadenced observations in *UBVRI* bands were obtained by AZT. The Konkoly observations were obtained in *BVRI* bands. Data from ObsN were obtained in *BVRI* and *gr* bands. The entire dataset covers phases from MJD 58286.89 (Jun. 17.89, 2018) to MJD 58348.74 (Aug. 18.74, 2018). The earliest photometric data point comes from ObsN in *V*-band on MJD 58286.89, which is ~ 0.27 day earlier than that presented in Prentice et al. (2018). Besides the fast rise, the object faded very quickly. The late time photometry may be influenced by contamination from the galaxy. Thus for AZT, LCO and KT, we obtained reference images in each band in Mar. 2019, Oct. 2018, and Feb. 2019, respectively. The reference images were obtained in all corresponding bands except for the *U*-band of AZT. For TNT images, since the source is still bright during observations, the influence of the background is negligible. Although the observations continued after Aug. 18, 2018, the object became too faint to be distinguished from the background.

All *UBVRI* and *gri* images are pre-processed using standard IRAF² routines, which includes corrections for bias, flat field, and removal of cosmic rays. To remove the contamination from the host galaxy, we applied template subtraction to the AZT, LCO and KT images. Note that the *U*-band images were not host subtracted. The instrumental magnitudes of both AT2018cow and the reference stars were then measured using the standard point spread function (PSF). And then the instrumental magnitudes were converted to standard Johnson and SDSS *gri*-band magnitudes using the zero points and color terms of each telescope. The resultant magnitudes are listed in Tab. 1. We also include the early photometry from Prentice et al. (2018) for comparison. The light curves are shown in Fig. 1.

Table 1. Portion of optical photometric observations of AT2018cow.

MJD	mag.	mag. error	band	Telescope/reference
58285.4400	14.700	0.100	o	Smartt et al. (2018)
58286.1950	14.320	0.010	i	Fremling (2018)
58286.8880	13.695	...	V	ObsN
58287.1130	13.593	...	V	ObsN
58287.1500	13.400	0.050	g	Prentice et al. (2018)
58287.1500	13.800	0.100	r	Prentice et al. (2018)
58287.1500	14.100	0.100	i	Prentice et al. (2018)
58287.4440	13.674	...	V	ObsN
58287.9270	13.771	...	V	ObsN
58287.9400	14.021	...	I	ObsN
58287.9460	13.926	...	r	ObsN
58287.9520	13.742	...	V	ObsN
58287.9540	13.692	...	B	ObsN
58287.9540	13.692	...	g	ObsN
58287.9750	13.725	...	R	ObsN
58288.0677	13.809	0.021	B	LCO
58288.0677	13.939	0.013	V	LCO
58288.0677	13.787	0.011	g	LCO
58288.0677	14.573	0.016	i	LCO
58288.0677	14.295	0.017	r	LCO

It can be seen that AT2018cow rises to a peak at MJD \sim 58287.0 in *V*, *R* and *I* bands, where the light curves are better sampled around the peak. The lat-

² IRAF is distributed by the National Optical Astronomy Observatories, which are operated by the Association of Universities for Research in Astronomy, Inc., under cooperative agreement with the National Science Foundation (NSF).

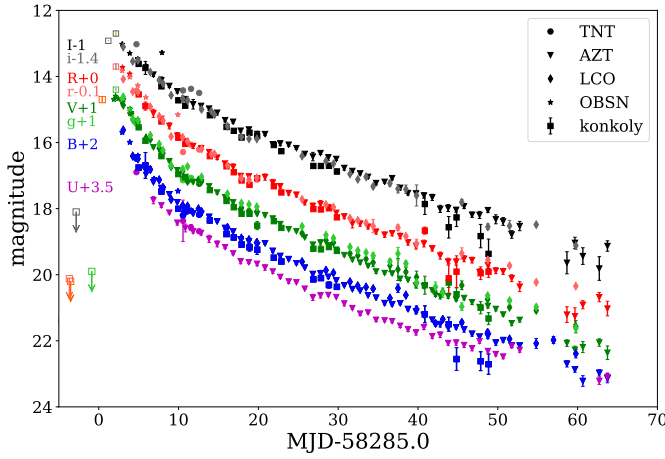


Figure 1. Light curves obtained from various telescopes. Discovery magnitude in *orange*-band from Smartt et al. (2018) (orange) and early follow-up photometry from Fremling (2018) and Prentice et al. (2018) are also plotted as empty squares. The pre-discovery detection limits are from Fremling (2018) and Prentice et al. (2018). The magnitudes in different bands are shifted for better display.

est non-detection limit is on MJD 58284.13 in *g*-band (Prentice et al. 2018), so the rise time of AT2018cow is less than 2.9 days. If we take the median of the first detection (i.e. discovery by ATLAS) MJD 58285.44 and the latest non-detection (i.e. MJD 58284.13) as the first light time, then the rise time is ~ 2.2 days. We apply an explosion time on $\text{MJD}=58284.79 \pm 0.66$ throughout this paper. This rise time is too short compared to supernovae, which usually have rise time of more than 10 days. After the peak, the light curves decline as fast as 0.33 mag d^{-1} , 0.27 mag d^{-1} , 0.22 mag d^{-1} , within the first 10 days in *V*, *R* and *I*-bands, respectively.

2.2. Optical Spectroscopic Observations

Our first spectrum was taken at Jul. 21, 2018 by the 2.16-m telescope at Xinglong Observatory of NAOC (hereafter XLT). A total of 31 spectra were collected

with different telescopes, including the XLT, the 2-m Faulkes Telescope North (FTN) of the Las Cumbres Observatory network, and the 9.2-m Hobby-Eberly Telescope (HET). The details of the spectroscopic observations are listed in Tab. 2.

All spectra were reduced using the standard IRAF routines, which involves corrections for bias, flat field, and removal of cosmic rays. The Fe/Ar and Fe/Ne arc lamp spectra obtained during the observation nights are used to calibrate the wavelength of the spectra, and standard stars observed on the same night at similar airmasses as the supernova were used to calibrate the flux of spectra. The spectra were further corrected for continuum atmospheric extinction during flux calibration using mean extinction curves obtained at Xinglong Observatory and Haleakala Observatory in Hawaii, respectively. Moreover, telluric lines were removed from the spectra of XLT and FTN. We recalibrated the fluxes of the spectra to the multi-band photometry data. The UV data from Perley et al. (2019) are included in the recalibration process. The recalibrated spectra are shown in Fig. 2.

On Sep. 17, 2019, when AT2018cow already faded away in the host galaxy, a spectrum was obtained at the site of AT2018cow by HET. There are some narrow absorption lines in the resultant spectrum, which are an artifact of data reduction. HET LRS2 is an IFU spectrograph having 280 individual fibers packed close together in a rectangular pattern, with a field-of-view of $12'' \times 6''$, which is smaller than the size of the host galaxy of AT2018cow. Since the data reduction pipeline determines the background by combining the fibers having the lowest flux level, the background will necessarily contain some of the galaxy features. Thus the spectra show some fake absorption lines resulting from subtraction of the emission lines from other faint part of the host galaxy. These fake lines are manually removed from the spectrum. A detailed analysis on this spectrum is presented in Sec. 4.

Table 2. Log of optical spectroscopy of AT2018cow.

UT	MJD	Telescope	Wav. range (\AA)	Instrument	Exposure time (s)
2018/06/21.58	58290.58	XLT	3970-8820	BFOSC	2400
2018/06/22.32	58291.32	HET	3640-10298	LRS2	300
2018/06/23.64	58292.64	XLT	3970-8820	BFOSC	2400
2018/06/24.50	58293.50	FTN	3500-10000	FLOYDS	1200

Table 2 continued

Table 2 (*continued*)

UT	MJD	Telescope	Wav. range (Å)	Instrument	Exposure time (s)
2018/06/26.30	58295.30	HET	3640-10300	LRS2	500
2018/06/26.39	58295.39	FTN	3500-10000	FLOYDS	1200
2018/06/26.54	58295.54	XLT	3970-8820	BFOSC	1200
2018/06/27.57	58296.57	XLT	3970-8820	BFOSC	2400
2018/06/28.35	58297.35	FTN	3500-10000	FLOYDS	1200
2018/06/28.55	58297.55	XLT	3970-8820	BFOSC	1200
2018/06/30.38	58299.38	FTN	3500-10000	FLOYDS	1200
2018/07/01.57	58300.57	XLT	3970-8820	BFOSC	1500
2018/07/04.48	58303.48	FTN	3500-10000	FLOYDS	1200
2018/07/06.43	58305.43	FTN	3500-10000	FLOYDS	2700
2018/07/08.37	58307.37	FTN	3500-10000	FLOYDS	2700
2018/07/10.33	58309.33	FTN	3500-10000	FLOYDS	2700
2018/07/11.41	58310.41	FTN	3500-10000	FLOYDS	2700
2018/07/12.25	58311.25	HET	6440-10300	LRS2	1000
2018/07/13.32	58312.32	FTN	3500-10000	FLOYDS	2700
2018/07/14.35	58313.35	FTN	3500-10000	FLOYDS	2700
2018/07/15.25	58314.25	HET	3640-6970	LRS2	800
2018/07/16.31	58315.31	FTN	3500-10000	FLOYDS	2700
2018/07/17.35	58316.35	FTN	3500-10000	FLOYDS	2700
2018/07/19.35	58318.35	FTN	3500-10000	FLOYDS	3600
2018/07/22.28	58321.28	FTN	3500-10000	FLOYDS	3600
2018/07/24.34	58323.34	FTN	3500-10000	FLOYDS	3600
2018/07/25.32	58324.32	FTN	3500-10000	FLOYDS	3600
2018/07/26.34	58325.34	FTN	3500-10000	FLOYDS	3600
2018/07/31.37	58330.37	FTN	4800-10000	FLOYDS	3600
2018/08/03.25	58333.25	FTN	3500-10000	FLOYDS	3600
2018/08/14.18	58344.18	HET	3640-8300	LRS2	1800
2019/09/17.09	58743.09	HET	3640-10200	LRS2	1800

3. OBSERVATIONAL PROPERTIES

3.1. *Light Curves and Color Evolution*

The light curves of AT2018cow show much faster evolution than other optical transients. In Fig. 3 we compare the V -band light curves of AT2018cow with other SNe of different subtypes, including the peculiar fast-evolving transient KSN2015K (Rest et al. 2018). One can see that both the rise and decline of AT2018cow are faster than any other known fast-evolving supernovae. The rise time is very close to KSN2015K, while AT2018cow is about 2 mags brighter. Most SLSNe have much slower evolution so we do not show them in the plot. AT2018cow is close to the type Ibn SN iPTF15ul (Hosseinzadeh et al. 2017) in peak luminosity, while it is similar to the type Ibn SN 2006jc in terms of fast decline

after the peak. It should be noted that the high luminosity as well as the rapid evolution seen in AT 2018cow lie in the range of SNe Ibn.

During our observations, AT2018cow maintains very blue color (i. e. $B - V \sim -0.1$ mag, Fig. 4). Thus, it should suffer little reddening from its host galaxy. This can also be verified by the absence of Na I D absorption line in the spectra. We only consider the Galactic extinction of $E(B - V) = 0.08$ (Schlafly & Finkbeiner 2011) for AT2018cow, and ignore the host extinction in this paper. As also proposed by Perley et al. (2019), the photospheric temperature of AT2018cow is as high as $\sim 30,000$ K near the maximum light, and is still as high as $\sim 14,000$ K at ~ 50 days after discovery. This is not seen in any other optical transients ever discovered. For supernovae, the photospheric temperature can be high in early times but usually cools down to

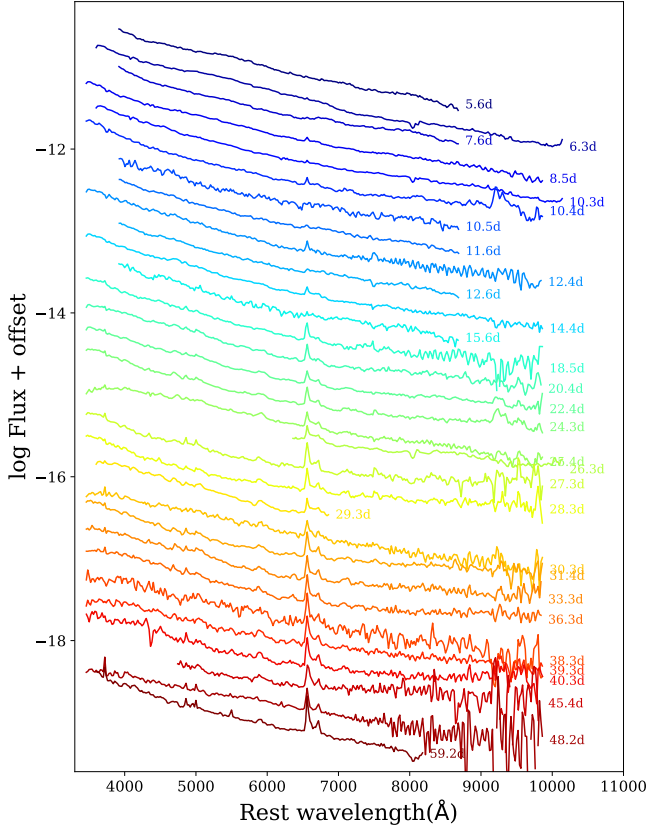


Figure 2. Optical spectra of AT2018cow. The numbers indicate days since MJD 58285. Host galaxy emissions are not removed. The data are smoothed by a bin of 20 Å for better display.

~ 5000 K in a few weeks after explosion, since the energy source is not strong enough to maintain a very high temperature. So the color of normal SNe will become red in late phases. In Fig. 4 we show the $B - V$ color evolution of AT2018cow in comparison with other SNe. The color evolution of AT2018cow resembles that of SN 2006jc. Assuming a blackbody SED shape, the spectra of SN 2006jc also seem to present unusually high effective temperature, $\sim 15,000$ K on day 8, then the temperature grows to 25,000 K on day 25 and drops to 15,000 K around day 60. The temperature decreases to $\sim 3,500$ K and then keeps flat after day 80. Nevertheless, the interaction and blending of iron lines may indeed contribute to the high temperature.

Another interesting point is that the photospheric radius seems to be decreasing since the very beginning, unlike that of normal SNe, which will increase before

peak and then decrease as a result of the expansion and dilution of the ejecta. The absence of an expansion phase is the main problem of the supernova origin for AT2018cow.

3.2. Spectral Evolution: Signatures of Interaction

The spectra of AT2018cow are characterized by featureless blue continuum in the first ~ 10 days after discovery, and then some broad emission features emerge later, with possible contaminations from the host galaxy. Featureless and blue spectra are common in SNe due to high photospheric temperature at early phases. Then spectral lines appear as the temperature decreases. We create normalized spectra of AT2018cow from the observed spectra by subtracting and deviding the best fit single blackbody continuum of each spectrum. In the first 10 days, the spectra are characterized by a wide feature near 5000\AA , as shown in Fig. 5. Later on, many broad emission lines emerge, overlapped with many narrow and strong emission lines. And there is flux excess in the red end, which is probably due to dust emission in later phases. As proposed by Fox & Smith (2019), the spectra of AT2018cow might have shown signatures of circumstellar interaction (CSI) like SNe Ibn and IIn. While the typical features of CSI are narrow emission lines of H and He. The last spectrum taken by HET shows many narrow emission lines ($\text{FWHM} \approx 4\text{\AA}$) which are apparently from the background host galaxy. Although other spectra of AT2018cow do show strong and broader $\text{H}\alpha$ lines since day 8 (Fig. 2), it is quite possible that the lines of H are from the host galaxy, not AT2018cow. The reason is that those spectra do not have such high resolution as that in HET spectrum, so the narrow lines are broadened. To figure out whether the narrow emission lines are from the host galaxy or AT2018cow, we measured the FWHMs of $\text{H}\alpha$ line in each spectrum and compared it with other lines in the same spectrum. The results show that the width of $\text{H}\alpha$ lines are only slightly broader than (by less than 10\AA , within the uncertainty) other narrow lines such as [NII] and [SII], indicating that they are probably from the host galaxy. Thus we conclude that there is no significant narrow emissions of H in AT2018cow.

To better look into the spectral features of AT2018cow at $t > 10$ days, we carefully subtracted the narrow emission lines of $\text{H}\alpha$, [NII] $\lambda 6548, 6583$ and [SII] $\lambda 6730, 6716$ from the spectra. For the spectra taken from ~ 10 days to ~ 59 days after discovery, we identify shallow and broad emission lines that can be attributed to HI, HeI, HeII, OI, OIII and CIII lines (as shown in Fig. 6). The OI, OIII, CIII and HeII lines dissipated after around day 45. The peaks of these lines are all slightly red-

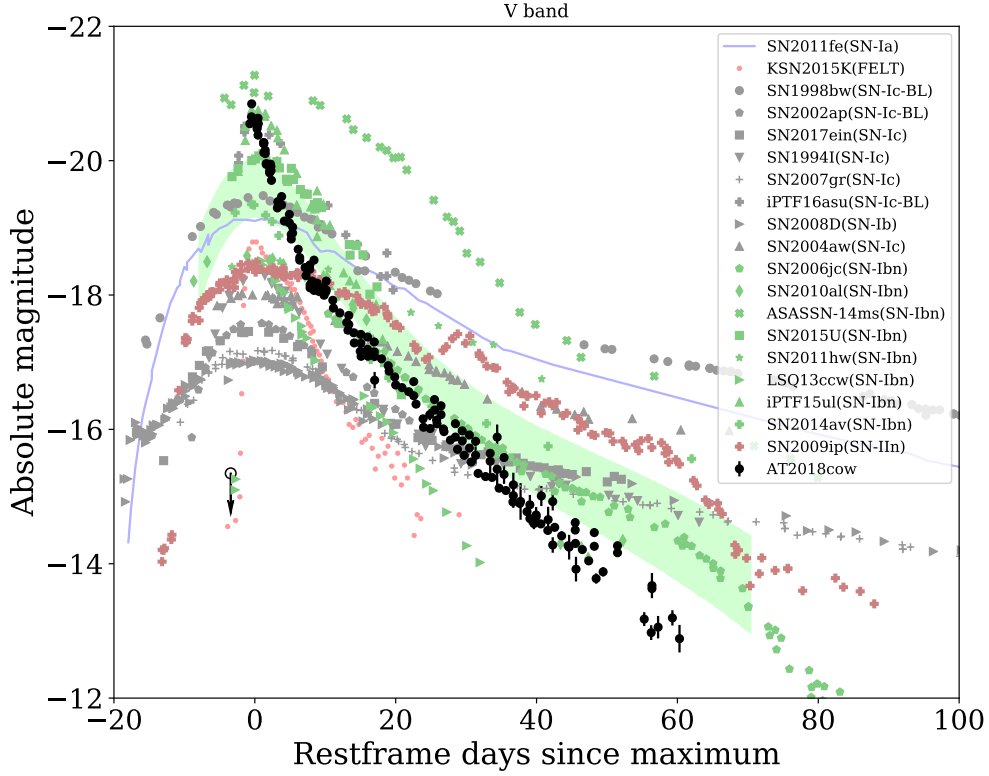


Figure 3. The V-band light curves of AT2018cow compared with other optical transients. Different colors are used to distinguish object types. The green shaded area shows the template R-band light curves of SNe Ibn from Hosseinzadeh et al. (2017). Data references: SN 2011fe (Zhang et al. 2016), KSN2015K (Rest et al. 2018), SN 1998bw (Galama et al. 1998; Sollerman et al. 2000; McKenzie & Schaefer 1999), SN 2002ap (Foley et al. 2003), SN 2017ein (Xiang et al. 2019; Van Dyk et al. 2018), SN 1994I (Richmond et al. 1996; Yokoo et al. 1994), SN 2007gr (Chen et al. 2014), iPTF16asu (Whitesides et al. 2017), SN 2008D (Mazzali et al. 2008; Modjaz et al. 2009; Bianco et al. 2014; Brown et al. 2014), SN 2004aw (Taubenberger et al. 2006), SN 2006jc (Bianco et al. 2014; Brown et al. 2014; Drout et al. 2011), SN 2010al (Hicken et al. 2017; Brown et al. 2014), ASASSN-14ms (Wang, et al. 2020, in prep.), SN 2015U (Shivvers et al. 2016; Tsvetkov et al. 2015), SN 2011hw (Brown et al. 2014; Smith et al. 2012b), LSQ13ccw (Smartt et al. 2015), iPTF15ul (Hosseinzadeh et al. 2017), SN 2014av (Pastorello et al. 2016), SN 2009ip: Mauerhan et al. (2013); Smartt et al. (2015). Part of the reference data are obtained via the Open Supernova Catalog (Guillochon et al. 2017).

shifted by up to 2000 km s^{-1} . The emission lines of AT2018cow are much broader than most SNe Ibn and IIn. The HeI $\lambda 5876$ line has an FWHM of $\sim 300 \text{ \AA}$ ($v \sim 15,000 \text{ km s}^{-1}$) at day 14, which is one magnitude higher than that of most SNe Ibn ($v \sim 1000 \text{ km s}^{-1}$). In late phases, the broad lines become narrower, with the FWHM decreasing to $\sim 3000 \text{ km s}^{-1}$ on day 59. Meanwhile, these broad emission lines are redshifted with velocities decreasing from $\sim 1800 \text{ km s}^{-1}$ when they first emerge, to hundreds of km s^{-1} in late phases. In the region of $\text{H}\alpha$, there is a broad emission line, which should be a blending of $\text{H}\alpha$ and HeI $\lambda 6678$. This line is seen getting narrower over time and splitted into two lines since $t \sim 30$ day, and the peaks moves to the rest wavelength. In addition to the long existing broad emission

lines, weak and narrow ($\text{FWHM} \sim 800\text{--}1000 \text{ km s}^{-1}$) HeI $\lambda 6678$ line emerged in the spectra since $t \sim 20$ days. This narrow line is certain to be from AT2018cow, as it does not appear in the spectrum of the host galaxy. To conclude, the broad emission lines of highly ionized elements (CIII, OIII) indicate that there is possible CSM interaction at very early time ($t < 10$ days). And the appearance of narrow He emission lines in late times ($t > 20$ days) implies the existence of another distant CSM formed around the progenitor object.

It is natural to think of an interacting SN picture for AT2018cow. Fox & Smith (2019) found the similarity between AT2018cow and some SNe Ibn and SNe IIn. Here we argue that although AT2018cow show signatures of interaction similar to SNe Ibn and SNe IIn,

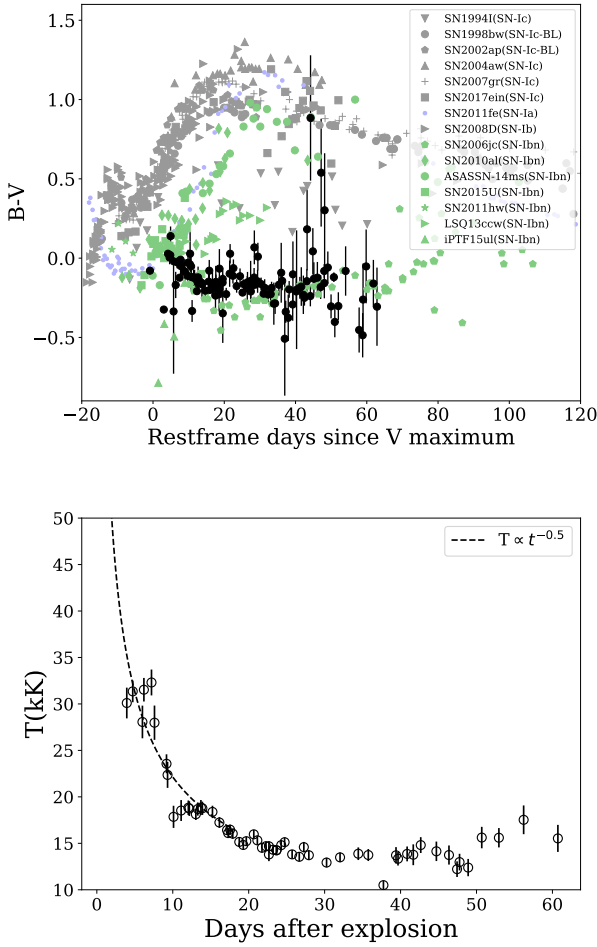


Figure 4. *Upper:* $B - V$ evolution of AT2018cow, in comparison with other well observed SNe. Symbols and references are the same as in Fig. 3. *Lower:* temperature evolution of AT2018cow. The dashed line shows the estimation of the early temperature as $T \propto t^{-0.5}$, which is used to estimate the early time bolometric luminosity (see Sec. 5).

its spectral evolution is quite different from that of SNe Ibn and IIn. In Fig. 7 we show the spectral evolution of AT2018cow compared with some well observed SNe Ibn, SN 2006jc (Pastorello et al. 2007; Smith et al. 2008), SN 2015U (Pastorello et al. 2015a; Shivvers et al. 2016) and SN 2002ao (Pastorello et al. 2008a), and a typical SN IIn 2010jl (Smith et al. 2012c; Zhang et al. 2012). From Fig. 7 we can see the diversity of SNe Ibn. AT2018cow seems to have different spectral features from any other interacting SNe, as it has weaker lines at all phases. At earlier phases AT2018cow is characterized by blue featureless continuum like that seen in some CCSNe as a result of high temperature, i. e. SN 2015U from our comparison sample. While SN 2015U shows a narrow P-cygni absorption fea-

ture, indicating the recombination of He in the CSM (Shivvers et al. 2016). Note that the emission lines of AT2018cow emerged at later phases, and are much weaker compared to SN 2006jc and SN 2002ao. Moreover, the Ca lines are very strong in SN 2006jc and SN 2015U, but are weak in AT2018cow. At late times, AT2018cow show similarities to SN 2002ao, both being dominated by broad lines. While P-cygni absorption of HeI lines are present in SN 2002ao, and the lines are stronger. The line velocity of HeI at $t \sim +24$ d is $\sim 8500 \text{ km s}^{-1}$ for SN 2002ao, slightly higher than AT2018cow ($\sim 7000 \text{ km s}^{-1}$). SN 2002ao is claimed as 06jc-like, which are proposed as Wolf-Rayet (WR) stars exploded in a He-rich CSM (Pastorello et al. 2008a). Although SNe Ibn and IIn are distinguished by the strength of the H emission lines, there are some transitional objects which show roughly equal strength of H and He emission lines, for example SN 2005la (Pastorello et al. 2008b) and SN 2011hw (Smith et al. 2012b; Pastorello et al. 2015b).

In most interacting supernovae, like SNe IIn and Ibn, the emission lines have velocities in range of tens to a few thousand km s^{-1} , depending on the wind velocities of the progenitor stars. The wind velocities are related to the type of the progenitor stars. At same metallicities, stars with larger initial masses are expected to have stronger stellar winds therefore higher wind velocities when they evolve to the end of life (see Smith 2014 and references therein). Some of the objects show intermediate width emission lines ($1000 \text{ km s}^{-1} < v < 4000 \text{ km s}^{-1}$), like SN 2006jc. In spectra of SN 2006jc, the bluer He lines show narrow P-Cygni profiles, while the redder He lines show an intermediate width emission component ($\text{FWHM} \approx 3000 \text{ km s}^{-1}$) (Foley et al. 2007). The broad emission features in AT2018cow are apparently different from the spectral features in ordinary SNe II. The lack of absorption features implies that AT2018cow is possibly more similar to SNe IIn/Ibn, rather than SNe IIP/IIL. While the velocities of the broad emission component in AT2018cow ($v \sim 10,000 \text{ km s}^{-1}$) are much higher than normal SNe Ibn/IIn. The lack of narrow emission lines in AT2018cow and relatively weak lines make it unique among interacting SNe. While this is not an argument against the interacting SN origin of AT2018cow, because spectral diversity is seen in other SNe Ibn and SNe IIn (e.g., Hosseinzadeh et al. 2017). Absence of narrow lines might be resulted from a closely located CSM which was immediately swept up by the shock within a short time period.

4. HOST GALAXY ENVIRONMENT

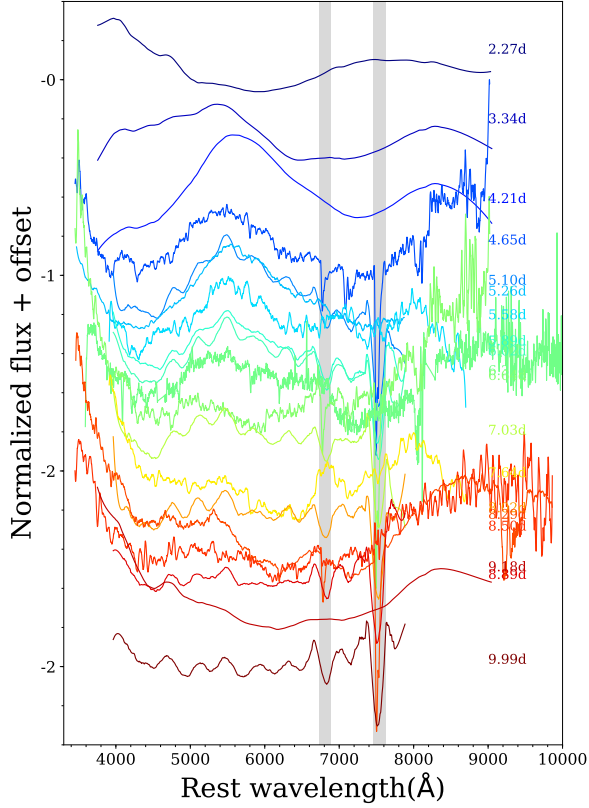


Figure 5. Normalized spectra of AT2018cow in the first 10 days. The shaded areas mark the region of telluric lines.

We notice that the spectra of AT2018cow are almost featureless at early phases ($t < 10$ d). Later on the spectra are some broader features overlapped with many narrow emission lines which are most probably due to the emission from the background galaxy. We obtained a spectrum of the host at the location of AT2018cow with the 9.2-m HET on Sep. 17, 2019 (corresponding to ~ 460 days after discovery), as shown in Fig. 8.

The spectrum is characterized by that of a typical HII region, which implies that this region is currently at gas phase and star-forming. One can see strong emission lines of H, He, N, S and O, and a NaI D absorption line at the rest wavelength of the Milky Way. With this spectrum, we are able to measure the intensities of the emission lines and then derive the properties of the local environment. Following Curti et al. (2017), we get a local metallicity of $12 + \log(\text{O}/\text{H}) \sim 8.65 \pm 0.07$, which is solar-like and among the range of other SNe Ibn (Pastorello et al. 2016). The star formation rate (SFR) can be derived from the luminosity of the $\text{H}\alpha$ emission line, for

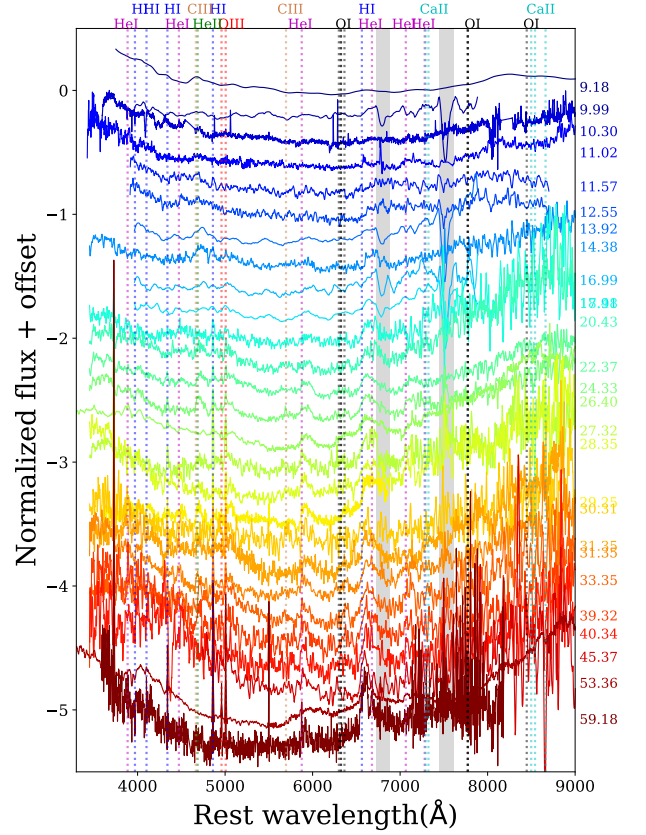


Figure 6. Normalized spectra of AT2018cow after 10 days since discovery. The spectra are normalized and the narrow emission lines from the host galaxy in the region around $\text{H}\alpha$ in spectra of AT2018cow are manually subtracted for better view. The numbers on the right mark the time in days since discovery (MJD 58285).

which we measured as $L(\text{H}\alpha) \approx 1.82 \times 10^{39} \text{ erg s}^{-1}$. This is consistent with the result from Lyman et al. (2020) $L(\text{H}\alpha) \approx 1.35 \times 10^{39} \text{ erg s}^{-1}$ at the site of AT2018cow, considering that we applied a larger distance. Using the conversion factor given in Sullivan et al. (2001), we get $\text{SFR}(\text{H}\alpha)_{\text{local}} \approx 0.015 M_{\odot} \text{ yr}^{-1}$. We also examine the $[\text{OII}]\lambda 3727$ line, and get $L([\text{OII}]) \approx 8.76 \times 10^{38} \text{ erg s}^{-1}$. With the relation given in Kennicutt (1998), we get $\text{SFR}([\text{OII}])_{\text{local}} \approx 0.012 M_{\odot} \text{ yr}^{-1}$, which is consistent with that from $\text{H}\alpha$ line. To get more information of the local environment of AT2018cow, we use Firefly (Wilkinson et al. 2017) to fit the spectrum with stellar population models. The input models are two M11 libs: MILES and STELIB (Maraston & Strömbäck 2011), and initial mass function ‘Kroupa’ (Kroupa 2001) is adopted in the fit. Fig. 8 shows the best fit spectra, from which

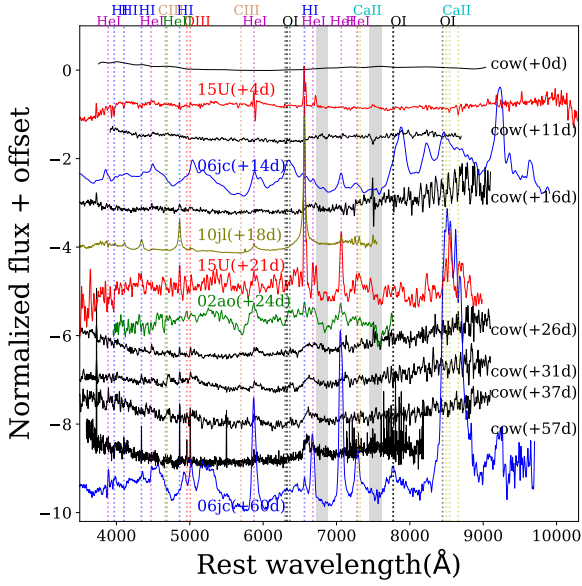


Figure 7. Normalized spectra of AT2018cow compared with other supernovae. All spectra are normalized by the fitted blackbody continuum. The numbers in the brackets are the phases relative to V -band maximum, which for AT2018cow we adopt MJD 58287. The narrow $H\alpha$ lines in spectra of AT2018cow are manually subtracted for better view.

we get a stellar mass of $M_\star \sim 5 \times 10^6 M_\odot$. Combining the above SFR and stellar mass information, we can get a local specific star formation rate (sSFR) as $\log(\text{sSFR})_{\text{local}} \sim -8.5 \text{ (yr}^{-1}\text{)}$.

The Sloan Digital Sky Survey (SDSS; Abolfathi et al. 2018) has taken one spectrum at the center of the host galaxy of AT2018cow on MJD 53566. As the HET spectrum we obtained only provides the local information, we also use the SDSS spectrum to measure the above corresponding parameters for the whole galaxy. The resulting metallicity is the same as that measured from the HET spectrum spotted at the site of AT2018cow, while the SFR is measured as $\text{SFR}(H\alpha)_{\text{center}} \approx 0.008 M_\odot \text{ yr}^{-1}$ if we do not consider any host extinction. The Firefly fit shows that the stellar mass of the nucleus is $M_\star \sim 2.6 \times 10^8 M_\odot$. We caution that the SDSS spectrum only includes the flux from the galaxy center, thus the SFR is expected to be lower. For the whole galaxy, we refer to the results from other studies. Perley et al. (2019) and Lyman et al. (2020) found stellar mass and SFR in good agreement with each other, although they adopted different distances. At $D_L=63 \text{ Mpc}$, stellar masses in these two studies become $M_\star \approx 1.56 \times 10^9 M_\odot$ and $1.85 \times 10^9 M_\odot$, respectively. And the SFR from Lyman et al. (2020) becomes $0.20 M_\odot \text{ yr}^{-1}$. In the following discussion, we adopt

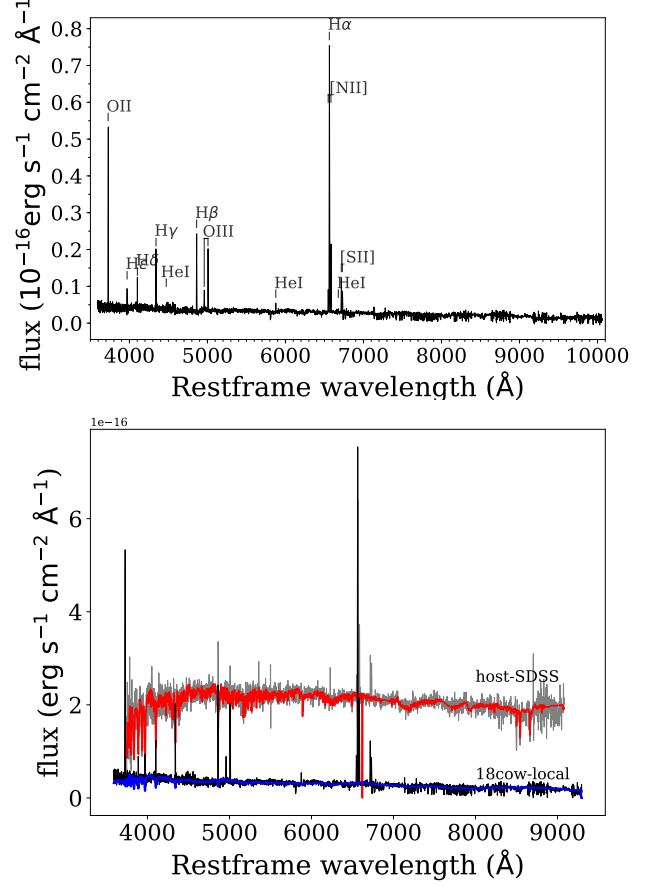


Figure 8. Upper panel: The spectrum taken at the location of AT2018cow. Lower panel: Firefly fitting of the host spectra at the site of the object and galaxy center. The over-plotted colored lines are the best fit models of Firefly.

an average of these results, i.e. $M_\star \approx 1.70 \times 10^9 M_\odot$, $\text{SFR} \approx 0.21 M_\odot \text{ yr}^{-1}$, and $\log(\text{sSFR}) \approx -9.88 \text{ (yr}^{-1}\text{)}$.

The host environment may provide a clue to the physical origin of AT2018cow. We compare the host environment parameters with other well studied transients, including type Ia supernovae (SNe Ia, Smith et al. 2012a; Galbany et al. 2014), core-collapse supernovae (CCSNe, Svensson et al. 2010; Galbany et al. 2014), superluminous supernovae (SLSNe, Angus et al. 2016), and gamma-ray bursts (GRBs, Svensson et al. 2010). As shown in Fig. 9, the host galaxy of AT2018cow is located among SNe Ia, CCSNe and GRBs, but away from the SLSNe group. The host galaxy of AT2018cow has stellar mass close to the median of GRBs, but at the lower end of the SNe group, except for SLSNe. We can not say for sure which group it should belong to, and it is likely that AT2018cow is distinct from SLSNe, although AT2018cow has a peak luminosity comparable to them. Meanwhile, the local high SFR of AT2018cow

may imply that AT2018cow is probably originated from a massive star.

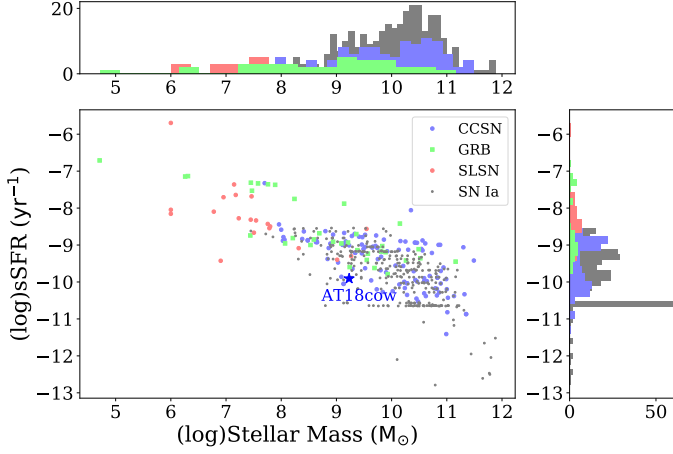


Figure 9. The host-galaxy parameters of AT2018cow compared with other types of transients.

5. MODELING THE RAPID EVOLVING LIGHT CURVES

The physical interpretation of AT2018cow is still in debate, although there are already several papers trying to uncover its physical origin. The radioactive decay of ^{56}Ni is a well known energy source for supernovae (Arnett 1982). The bolometric light curve of AT2018cow can not be powered by pure ^{56}Ni , as the peak luminosity would require an ejected ^{56}Ni mass of $\sim 6 M_{\odot}$ but a low ejecta mass $< 1 M_{\odot}$. In the above analysis, we find high resemblance of the light curves of AT2018cow to that of SNe Ibn, and signatures of CSI are found in the spectra, so we try to fit the light curves of AT2018cow using the CSI model. The fast-declining and luminous bolometric light curve of SN 2006jc has been successfully modeled by CSI models (e.g., Chugai 2009; Tominaga et al. 2008). The rapid declining light curves can be related to the early shock-cooling from the progenitor envelope. Since the progenitor has lost most of its hydrogen envelope, the shock-cooling should be weak and short for the core-collapse of a massive star. Another reasonable interpretation is the interaction of the supernova ejecta with the surrounding circumstellar medium (CSM). This can be supported by the emission lines in the spectra (see Sec. 3.2).

We construct the bolometric light curves by integrating the UV and optical flux (the UV data are taken from Perley et al. 2019), and then apply a model in which CSI is dominating the early time light curve. In

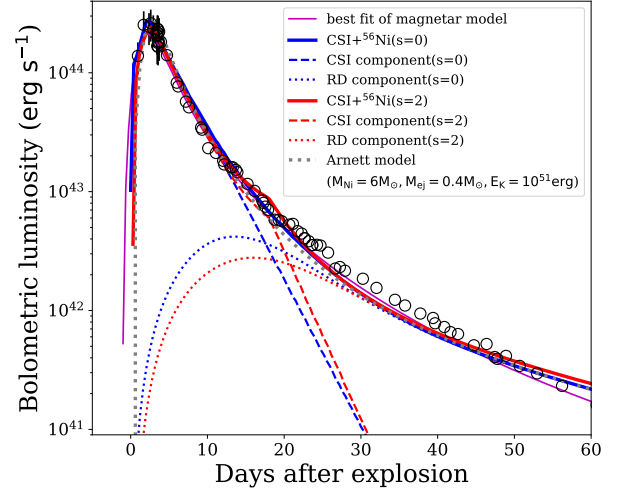


Figure 10. Bolometric light curve of AT2018cow. Best-fit models of CSI+RD with $s=0, 2$ are plotted in blue and red solid lines, respectively. The two components of the models are shown by dashed (CSI) and dotted (RD) lines, respectively. The best-fit magnetar model is plotted as a magenta solid line. A pure RD model is also shown in a grey dotted line as a reference.

order to constrain the fitting better, especially to obtain data before peak, we estimate the pre-peak bolometric luminosities based on the following assumptions: 1). the SED of AT2018cow is a blackbody; 2). the photometric temperature evolves as a power law $T \propto (t - t_0)^{-0.5}$, as we derived from the early temperature evolution. And then the bolometric luminosities before MJD 58288.44 are estimated using the single band photometry data. We adopt a hybrid model which includes ^{56}Ni powering and the interaction of the SN ejecta with a dense CSM with density profile as a power-law, i. e. $\rho_{\text{CSM}} \propto r^{-s}$, where the typical value of s is 2 and 0 (e.g., Chatzopoulos et al. 2012, 2013; Wang et al. 2019). In our model, the density distribution of the ejecta is uniform in the inner region ($\delta=0$), and follows a power-law ($\rho \propto r^{-12}$) in the outer region. The early fast rising light curve of AT2018cow is mainly powered by CSI, while the slower declining tail is dominated by radioactive decay (RD) of ^{56}Ni . We first consider the case of $s=2$, which corresponds to a steady-wind CSM. The best-fit light curve is shown in Fig. 10, and the fitted parameters are presented in Tab. 3. As shown in Fig. 10, our CSI+RD($s=2$) model can fit the observations quite well. The mass loss rate of the progenitor star can be estimated as $0.1(v_{\text{CSM}}/100 \text{ km s}^{-1}) M_{\odot} \text{ yr}^{-1}$, $\sim 1 M_{\odot} \text{ yr}^{-1}$ with $v_{\text{CSM}} \sim 1000 \text{ km s}^{-1}$. Margutti et al. (2019) also reach similar conclusion by analysing the optical and X-ray data. Such a mass loss rate is much higher than

that found from the radio observations of AT2018cow ($\dot{M} \sim 10^{-4} - 10^{-3} M_{\odot} \text{ yr}^{-1}$) (Ho et al. 2019 had a similar conclusion). If we set limit on the mass loss rate, the model can hardly fit the observations. Thus, we claim that the early bright and fast evolving light curve of AT2018cow can not be produced by CSI with a steady stellar wind.

We then try the other case where $s=0$, i. e. the density of the CSM is a constant. The fitting result is shown in Fig. 10, and the fitted parameters are presented in Tab. 3. As shown in Fig. 10, with $M_{\text{ej}} \approx 3.16 M_{\odot}$, $M_{\text{CSM}} \approx 0.04 M_{\odot}$, $M_{\text{Ni}} \approx 0.23 M_{\odot}$, the CSM+ ^{56}Ni ($s=0$) model can also provide a plausible fit for the observed bolometric light curve. The inferred inner radius of the CSM gives a constraint on the radius of the progenitor star $R < 3 R_{\odot}$, which is consistent with the typical size of WR stars. The CSM shell extends outwards to a radius of $8.70 \times 10^{13} \text{ cm}$ ($\approx 1200 R_{\odot}$), implying that the CSM was formed shortly prior to the explosion. Such a CSM shell can be produced by an episodic mass ejection from the progenitor star, like a luminous blue variable (LBV) or from a common-envelope episode of a binary system. Combining the mass and velocity of the ejecta, the kinetic energy of the ejecta can be estimated as $6.6 \times 10^{51} \text{ erg}$, several times higher than that of the ordinary SNe Ibc and rather similar to the broad lined SNe Ic (SN Ic-BL) (Lyman et al. 2016), which are found to be possibly associated with long gamma ray bursts (e.g. SN 1998bw (Iwamoto et al. 1998; Nakamura et al. 2001)). The high velocity of the ejecta might be connected to a relativistic jet.

Alternatively, the bolometric luminosity and effective temperature evolutions can be explained by a magnetar-powered model (Nicholl et al. 2017). Assuming that the opacities of ejecta are $\kappa = 0.2 \text{ cm}^2 \text{ g}^{-1}$ for the optical photon and $\kappa_{\text{mag}} = 0.013 \text{ cm}^2 \text{ g}^{-1}$ for the magnetar wind, respectively, the best-fit parameters for this model are $t_0 = 58283.4$, $M_{\text{ej}} = 0.1 M_{\odot}$, $v_{\text{ej}} = 2.72 \times 10^4 \text{ km s}^{-1}$, $P = 4.5 \text{ ms}$ and $B = 1.11 \times 10^{14} \text{ G}$, where P and B are the initial spin period and magnetic field strength of the nascent magnetar, respectively. We caution that the best-fit $M_{\text{ej}} = 0.1 M_{\odot}$ is the lower limit of the magnetar model in our fitting program. If no limit is given, the fitting tends to find a significantly lower value to fit the narrow light curve better. This may imply that the magnetar-powered model requires a rather low ejecta mass for AT2018cow.

6. DISCUSSION: PROGENITOR PROPERTIES

In the previous section, we made analysis of the bolometric light curve of AT2018cow based on an assumption that it is a supernova origin. While we do not rule

Table 3. Parameters of the best fit CSM+ ^{56}Ni models for AT2018cow.

...	$s=0$	$s=2$
t_0	MJD 58284.5	MJD 58284.7
$M_{\text{ej}}(M_{\odot})$	3.16	1.69
x_0^a	0.63	0.76
$v_{\text{ej}}(\text{km s}^{-1})$	26000	13600
$M_{\text{Ni}}(M_{\odot})$	0.23	0.14
$M_{\text{CSM}}(M_{\odot})$	0.04	0.12
$r_{\text{CSM},\text{in}}(\text{cm})^b$	2.11×10^{11}	1.03×10^{13}
$r_{\text{CSM},\text{out}}(\text{cm})^c$	8.70×10^{13}	3.16×10^{14}
$\rho_{\text{CSM},\text{in}}(\text{g cm}^{-3})^d$	2.9×10^{-11}	5.6×10^{-10}
ϵ^e	0.22	0.65
κ	0.14	0.15
κ_{γ}	0.015	0.014

^aThe dimensionless radius of the division between inner and outer region of ejecta.

^bThe inner radius of CSM.

^cThe outer radius of CSM.

^dThe CSM density at $r_{\text{CSM},\text{in}}$.

^eThe radiation efficiency.

out other possibilities, especially the TDE origin. A main problem of the supernova origin for AT2018cow is that the process of an expanding photosphere is missing. In early phases, the photospheric velocity may be very high ($\sim 0.1c$) for AT2018cow in early phases. The photospheric radius keeps decreasing since very early time. This can be a clue for the interpretation as a TDE for AT2018cow. Although both Lyman et al. (2020) and Margutti et al. (2019) find no evidence of the connection between the site of AT2018cow and an IMBH. Nevertheless, one can notice that the measurements of photospheric radius start after the peak, probably suggesting that the expanding phase is not observed.

The magnetar-powered model can make a good fit to the bolometric light curve. The best-fit B and P of the central engine lies in the range of SLSNe (Lin et al. 2020 and references therein). Distinction between AT2018cow and SLSNe is the evolution timescale, which is related to the ejecta mass. Nicholl et al. (2017) found $M_{\text{ej}} \geq 2.2 M_{\odot}$ with an average of $4.8 M_{\odot}$. Besides, the low ejected mass ($M_{\text{ej}} \sim 0.1 M_{\odot}$) required by the magnetar model for AT2018cow is not likely favorable for a massive star, except for some really extreme cases. Some studies find that massive stars can be ultra-stripped by

binary interaction with a compact neutron star (Tauris et al. 2015). But in these cases, little H or He remains in the progenitor system, which is not consistent with the observed spectral features of AT2018cow. Thus, we disfavor the magnetar model for AT2018cow.

Our CSI+RD($s=0$) model makes a plausible fit to the bolometric light curve of AT2018cow. With $R < 3R_{\odot}$, the progenitor star is most likely to be a compact WR star. The ejected mass ($M_{\text{ej}} \approx 3M_{\odot}$) is lower than that predicted by single stellar evolution models (e.g., Georgy et al. 2012) but around the mean value of SNe Ibc (Lyman et al. 2016). This might be a result of binary interaction or episodic eruptive mass loss during the lifetime of massive stars. It is hard to derive the mass of the progenitor star simply from the ejecta mass, since the mass loss mechanisms of massive stars can be complicated and ambiguous.

In the case of $s=0$, the CSM can be dense shells formed by strong stellar winds of WR stars or an eruptive of LBV stars (Chevalier & Liang 1989; Dwarkadas 2011). According to our fitting result, with wind velocity of 100 km s^{-1} , the eruption started several months before core-collapse, and was possibly still on when exploding. The average mass loss rate is $\sim 0.15M_{\odot} \text{ yr}^{-1}$, or even higher if the wind velocity is higher, lying well in the range of LBV eruptions (Smith 2014). Such mass loss behaviour can be found in some SNe IIn and SNe Ibn (Gal-Yam et al. 2007; Taddia et al. 2015; Pastorello et al. 2015b; Kiewe et al. 2012; Moriya et al. 2014a). Under this scenario, the progenitor of AT2018cow might be a massive star which is during eruptive state. However, with $R < 3R_{\odot}$, the progenitor star is most likely to be H-poor or even He-poor, so is the CSM. While there is possibility that H and He are mixed into inner shells so that the progenitor can keep some H/He at core-collapse.

Meanwhile, binary interaction might dominate the evolution of massive stars, which are thought to be the progenitors of stripped envelope supernovae (SESNe). Mass loss can be quite efficient in binaries (Eldridge et al. 2017). SN 2006jc is a representative of interacting SNe originated from binary massive stars (Maund et al. 2016; Sun et al. 2020). In the binary scenario, the progenitors can be less massive stars, and the companion stars evolve slower so that they can keep their H/He envelopes. A common-envelope episode of a binary system can also form this dense CSM shell. The detection of H and He lines in the spectra of AT2018cow indicates that the CSM is not H-free. So it is quite possible that the CSM is from the companion star rather than the progenitor itself. The slightly redshifted peaks of the emission

lines in the spectra of AT2018cow suggest asymmetry of the CSM, in favor of the common-envelope picture.

The progenitor star could be a very massive star which have experienced violent mass loss due to pulsational ejection. Recently Leung et al. (2020) has proposed a scenario based on a pulsational pair-instability supernova (PPISN) model, concluding that the rapidly evolving light curve of AT2018cow can be explained by a $42 M_{\odot}$ He star exploding in a dense He-rich CSM ($M_{\text{CSM}} \sim 0.5 M_{\odot}$). The proposed model can fit the bolometric light curve well (at $t < 30$ days). However, the presence of H lines in the spectra of AT2018cow is inconsistent with the assumption that both the ejecta and CSM formed around AT2018cow should be H-poor. Leung et al. (2020) tested different compositions of the CSM and found that the amount of H in the CSM only has slight effect on the bolometric light curve. Our fitting result is in agreement with Leung et al. (2020) in terms of the density and size of the CSM, but we find much lower CSM mass. We do not assume any Ni-mixing, while Leung et al. (2020) assumes that Ni is fully mixed into the outer layers of the ejecta. Nevertheless, both models may be plausible. Our model can correspond to a massive progenitor in a binary system, while Leung et al. (2020) requires a very massive star, whose zero-age-main-sequence (ZAMS) mass is $80 M_{\odot}$. It is worth noting that Leung et al. (2019) claims that a massive He core can only be formed under low metallicity ($Z \leq 0.5Z_{\odot}$), which is inconsistent with our measurement of a solar-like metallicity environment for the progenitor of AT2018cow (see Sec. 4). This may imply that the progenitor of AT2018cow did not undergo PPI.

The fast evolving light curves of AT2018cow may be related to a very low ejecta mass, which is consistent with electron-capture supernovae (ECSNe) (Nomoto 1984, 1987; Nomoto & Kondo 1991; Moriya et al. 2014b). Stars with ZAMS mass of $\sim 8\text{--}12 M_{\odot}$ form degenerate cores of O, Ne and Mg, which are susceptible to electron capture, leading to core collapse. For KSN 2015K, an example of FELTs, Rest et al. (2018) prefers a CSI model, while Tolstov et al. (2019) has found that the collapse of an ONeMg star surrounded by an optically thick CSM can also explain the fast rise of the light curve. However, the progenitors of ECSNe are thought to be super-AGB stars, which have stellar winds with relatively low velocities ($\sim 10 \text{ km s}^{-1}$). According to theoretical predictions, ECSNe are usually faint and have low explosion energies (e.g., Kawabata et al. 2010; Botticella et al. 2009 and a most recent study Hiramatsu et al. 2020). Thus, the ECSN scenario is unlikely for AT2018cow.

7. SUMMARY

In this paper, we present our photometric and spectroscopic observations on the peculiar transient AT2018cow. The multi-band photometry covers from peak to ~ 70 days and spectroscopy ranges from 5 to ~ 50 days after discovery. The rapid rise ($t_r \lesssim 2.9$ days), luminous light curves ($M_{V,\text{peak}} \sim -20.8$ mag) and fast post-peak decline make AT2018cow stand out of any other optical transients. After a thorough analysis, we find that the light curves and color evolution show high resemblances to some SNe Ibn. With detailed analysis of the spectral evolution and line identifications, we find that AT2018cow shows similar properties to the interacting SNe, like SNe IIn and SNe Ibn. Some broad emission lines due to H I, He I, He II, C III, O I, and O III emerge at $t \sim 10$ days, with v_{FWHM} decreasing from $\sim 11,000 \text{ km s}^{-1}$ to $\sim 3000 \text{ km s}^{-1}$ at the end of our observations. At $t \sim 20$ days, narrow and weak He I lines ($v_{\text{FWHM}} \sim 800\text{--}1000 \text{ km s}^{-1}$) overlain on the broad lines. These emission lines are evidence of interaction between the ejecta and a H-rich CSM. Furthermore, we spotted the site of AT2018cow after it faded away and find that it has a solar-like metallicity. The host galaxy of AT2018cow has properties similar to those of GRBs and CCSNe, but is distinct from SLSNe and SNe Ia. High star formation rate at the site of AT2018cow implies that AT2018cow might originate from a massive star.

Based on the interpretation of a CSI supernova, we fit the bolometric light curves with CSI+RD models. We find that in order to produce the fast and bright early light curve of AT2018cow, the CSI model with a steady wind requires much larger mass loss rate than that derived from radio observations. While with a dense uniform CSM shell, the CSI+RD model can make plausible fit with best-fit parameters $M_{\text{ej}} \sim 3.16 M_{\odot}$, $M_{\text{CSM}} \sim 0.04 M_{\odot}$, $M_{\text{Ni}} \sim 0.23 M_{\odot}$. Such a CSM shell can be formed by eruptive mass ejection of LBVs immediately before core-collapse or common envelope ejection in binaries. With $Z \approx Z_{\odot}$, the progenitor is less likely to have undergone PPI. We conclude that the progenitor of AT2018cow is likely to be a less massive star in a binary system.

We acknowledge the support of the staff of the Xinglong 2.16 m and Lijiang 2.4 m telescope. This work

is supported by the National Natural Science Foundation of China (NSFC grants 12033003, 11761141001, and 11633002), and the National Program on Key Research and Development Project (grant no. 2016YFA0400803). This work was also partially supported by the Open Project Program of the Key Laboratory of Optical Astronomy, National Astronomical Observatories, Chinese Academy of Sciences. This work is partially supported by the Scholar Program of Beijing Academy of Science and Technology (DZ:BS202002). J.-J. Zhang is supported by the National Science Foundation of China (NSFC, grants 11403096, 11773067), the Key Research Program of the CAS (Grant NO. KJZD-EW-M06), the Youth Innovation Promotion Association of the CAS (grants 2018081), and the CAS “Light of West China” Program. X.L. was supported by the China Postdoctoral Science Foundation funded project (No: 2017m610866). This work makes use of the LCO network. J.B., D.A.H., and D.H. were supported by NSF grant AST-1911225, and NASA grant 80NSSC19kfl639. Research by S.V. is supported by NSF grants AST-1818176 and AST-2008108. We thank the staff of AZT for their observations and allowance of the use of the data.

JV and his group at Konkoly Observatory is supported by the project “Transient Astrophysical Objects” GINOP 2.3.2-15-2016-00033 of the National Research, Development and Innovation Office (NKFIH), Hungary, funded by the European Union. LK received support from the Hungarian National Research, Development and Innovation Office grant OTKA K-131508, and from the János Bolyai Research Scholarship of the Hungarian Academy of Sciences. AB has been supported by the Lendület Program of the Hungarian Academy of Sciences, project No. LP2018-7/2019. ZsB acknowledges the support provided by the Hungarian National Research, Development and Innovation Office (NKFIH), project No. PD-123910, and the support by the János Bolyai Research Scholarship of the Hungarian Academy of Sciences.

Software: ZrutyPhot (Mo et al. in prep.), IRAF (Tody 1993, 1986), Firefly (Wilkinson et al. 2017).

REFERENCES

- | | |
|--|---|
| <p>Abolfathi, B., Aguado, D. S., Aguilar, G., et al. 2018, ApJS, 235, 42</p> | <p>Angus, C. R., Levan, A. J., Perley, D. A., et al. 2016, MNRAS, 458, 84</p> |
|--|---|

- Arcavi, I., Wolf, W. M., Howell, D. A., et al. 2016, *ApJ*, 819, 35
- Arnett, W. D. 1982, *Astrophysical Journal*, 253, 785
- Bianco, F. B., Modjaz, M., Hicken, M., et al. 2014, *ApJS*, 213, 19
- Botticella, M. T., Pastorello, A., Smartt, S. J., et al. 2009, *MNRAS*, 398, 1041
- Brown, P. J., Breeveld, A. A., Holland, S., Kuin, P., & Pritchard, T. 2014, *Ap&SS*, 354, 89
- Chatzopoulos, E., Wheeler, J. C., & Vinko, J. 2012, *ApJ*, 746, 121
- Chatzopoulos, E., Wheeler, J. C., Vinko, J., Horvath, Z. L., & Nagy, A. 2013, *ApJ*, 773, 76
- Chen, J., Wang, X., Ganeshalingam, M., et al. 2014, *ApJ*, 790, 120
- Chevalier, R. A., & Liang, E. P. 1989, *ApJ*, 344, 332
- Chugai, N. N. 2009, *MNRAS*, 400, 866
- Curti, M., Cresci, G., Mannucci, F., et al. 2017, *MNRAS*, 465, 1384
- Drout, M. R., Soderberg, A. M., Gal-Yam, A., et al. 2011, *ApJ*, 741, 97
- Drout, M. R., Chornock, R., Soderberg, A. M., et al. 2014, *ApJ*, 794, 23
- Dwarkadas, V. V. 2011, *MNRAS*, 412, 1639
- Ehgamberdiev, S. 2018, *Nature Astronomy*, 2, 349
- Eldridge, J. J., Stanway, E. R., Xiao, L., et al. 2017, *PASA*, 34, e058
- Foley, R. J., Smith, N., Ganeshalingam, M., et al. 2007, *ApJL*, 657, L105
- Foley, R. J., Papenkova, M. S., Swift, B. J., et al. 2003, *PASP*, 115, 1220
- Fox, O. D., & Smith, N. 2019, *MNRAS*, 488, 3772
- Fremling, C. 2018, *The Astronomer’s Telegram*, 11738, 1
- Gal-Yam, A., Leonard, D. C., Fox, D. B., et al. 2007, *ApJ*, 656, 372
- Galama, T. J., Vreeswijk, P. M., van Paradijs, J., et al. 1998, *Nature*, 395, 670
- Galbany, L., Stanishev, V., Mourão, A. M., et al. 2014, *A&A*, 572, A38
- Georgy, C., Ekström, S., Meynet, G., et al. 2012, *A&A*, 542, A29
- Guillochon, J., Parrent, J., Kelley, L. Z., & Margutti, R. 2017, *ApJ*, 835, 64
- Hicken, M., Friedman, A. S., Blondin, S., et al. 2017, *ApJS*, 233, 6
- Hiramatsu, D., Howell, D. A., Van Dyk, S. D., et al. 2020, *arXiv e-prints*, arXiv:2011.02176
- Ho, A. Y. Q., Phinney, E. S., Ravi, V., et al. 2019, *ApJ*, 871, 73
- Hosseinzadeh, G., Arcavi, I., Valenti, S., et al. 2017, *ApJ*, 836, 158
- Howell, D. A. 2017, *Superluminous Supernovae*, ed. A. W. Alsabti & P. Murdin, 431
- Huang, F., Li, J.-Z., Wang, X.-F., et al. 2012, *Research in Astronomy and Astrophysics*, 12, 1585
- Iwamoto, K., Mazzali, P. A., Nomoto, K., et al. 1998, *Nature*, 395, 672
- Kawabata, K. S., Maeda, K., Nomoto, K., et al. 2010, *Nature*, 465, 326
- Kennicutt, Robert C., J. 1998, *ARA&A*, 36, 189
- Kiewe, M., Gal-Yam, A., Arcavi, I., et al. 2012, *ApJ*, 744, 10
- Kroupa, P. 2001, *MNRAS*, 322, 231
- Kuin, N. P. M., Wu, K., Oates, S., et al. 2019, *MNRAS*, 487, 2505
- Leung, S.-C., Blinnikov, S., Nomoto, K., et al. 2020, *ApJ*, 903, 66
- Leung, S.-C., Nomoto, K., & Blinnikov, S. 2019, *ApJ*, 887, 72
- Lin, W. L., Wang, X. F., Wang, L. J., & Dai, Z. G. 2020, *ApJL*, 903, L24
- Lyman, J. D., Bersier, D., James, P. A., et al. 2016, *MNRAS*, 457, 328
- Lyman, J. D., Galbany, L., Sánchez, S. F., et al. 2020, *MNRAS*, 495, 992
- Lyutikov, M., & Toonen, S. 2019, *MNRAS*, 487, 5618
- Maraston, C., & Strömbäck, G. 2011, *MNRAS*, 418, 2785
- Margutti, R., Metzger, B. D., Chornock, R., et al. 2019, *ApJ*, 872, 18
- Mauerhan, J. C., Smith, N., Filippenko, A. V., et al. 2013, *MNRAS*, 430, 1801
- Maund, J. R., Pastorello, A., Mattila, S., Itagaki, K., & Boles, T. 2016, *ApJ*, 833, 128
- Mazzali, P. A., Valenti, S., Della Valle, M., et al. 2008, *Science*, 321, 1185
- McKenzie, E. H., & Schaefer, B. E. 1999, *PASP*, 111, 964
- Modjaz, M., Li, W., Butler, N., et al. 2009, *ApJ*, 702, 226
- Moriya, T. J., Maeda, K., Taddia, F., et al. 2014a, *MNRAS*, 439, 2917
- Moriya, T. J., Tominaga, N., Langer, N., et al. 2014b, *A&A*, 569, A57
- Nakamura, T., Mazzali, P. A., Nomoto, K., & Iwamoto, K. 2001, *ApJ*, 550, 991
- Nicholl, M., Guillochon, J., & Berger, E. 2017, *ApJ*, 850, 55
- Nomoto, K. 1984, *ApJ*, 277, 791
- . 1987, *ApJ*, 322, 206
- Nomoto, K., & Kondo, Y. 1991, *ApJL*, 367, L19
- Pastorello, A., Smartt, S. J., Mattila, S., et al. 2007, *Nature*, 447, 829

- Pastorello, A., Mattila, S., Zampieri, L., et al. 2008a, *MNRAS*, 389, 113
- Pastorello, A., Quimby, R. M., Smartt, S. J., et al. 2008b, *MNRAS*, 389, 131
- Pastorello, A., Tartaglia, L., Elias-Rosa, N., et al. 2015a, *MNRAS*, 454, 4293
- Pastorello, A., Benetti, S., Brown, P. J., et al. 2015b, *MNRAS*, 449, 1921
- Pastorello, A., Wang, X. F., Ciabattari, F., et al. 2016, *MNRAS*, 456, 853
- Perley, D. A., Mazzali, P. A., Yan, L., et al. 2019, *MNRAS*, 484, 1031
- Planck Collaboration, Ade, P. A. R., Aghanim, N., et al. 2016, *A&A*, 594, A13
- Prentice, S. J., Maguire, K., Smartt, S. J., et al. 2018, *ApJL*, 865, L3
- Quimby, R. M., Kulkarni, S. R., Kasliwal, M. M., et al. 2011, *Nature*, 474, 487
- Rest, A., Garnavich, P. M., Khatami, D., et al. 2018, *Nature Astronomy*, 2, 307
- Richmond, M. W., van Dyk, S. D., Ho, W., et al. 1996, *AJ*, 111, 327
- Schlaafy, E. F., & Finkbeiner, D. P. 2011, *ApJ*, 737, 103
- Shivvers, I., Zheng, W. K., Mauerhan, J., et al. 2016, *MNRAS*, 461, 3057
- Smartt, S. J., Valenti, S., Fraser, M., et al. 2015, *A&A*, 579, A40
- Smartt, S. J., Clark, P., Smith, K. W., et al. 2018, *The Astronomer's Telegram*, 11727
- Smith, M., Nichol, R. C., Dilday, B., et al. 2012a, *ApJ*, 755, 61
- Smith, N. 2014, *ARA&A*, 52, 487
- Smith, N., Foley, R. J., & Filippenko, A. V. 2008, *ApJ*, 680, 568
- Smith, N., Mauerhan, J. C., Silverman, J. M., et al. 2012b, *MNRAS*, 426, 1905
- Smith, N., Silverman, J. M., Filippenko, A. V., et al. 2012c, *AJ*, 143, 17
- Sollerman, J., Kozma, C., Fransson, C., et al. 2000, *ApJL*, 537, L127
- Sullivan, M., Mobasher, B., Chan, B., et al. 2001, *ApJ*, 558, 72
- Sun, N.-C., Maund, J. R., Hirai, R., Crowther, P. A., & Podsiadlowski, P. 2020, *MNRAS*, 491, 6000
- Svensson, K. M., Levan, A. J., Tanvir, N. R., Fruchter, A. S., & Strolger, L. G. 2010, *MNRAS*, 405, 57
- Taddia, F., Sollerman, J., Fremling, C., et al. 2015, *A&A*, 580, A131
- Taubenberger, S., Pastorello, A., Mazzali, P. A., et al. 2006, *MNRAS*, 371, 1459
- Tauris, T. M., Langer, N., & Podsiadlowski, P. 2015, *MNRAS*, 451, 2123
- Tody, D. 1986, in *Proc. SPIE*, Vol. 627, *Instrumentation in astronomy VI*, ed. D. L. Crawford, 733
- Tody, D. 1993, in *Astronomical Society of the Pacific Conference Series*, Vol. 52, *Astronomical Data Analysis Software and Systems II*, ed. R. J. Hanisch, R. J. V. Brissenden, & J. Barnes, 173
- Tolstov, A., Nomoto, K., Sorokina, E., et al. 2019, *ApJ*, 881, 35
- Tominaga, N., Limongi, M., Suzuki, T., et al. 2008, *ApJ*, 687, 1208
- Tsvetkov, D. Y., Volkov, I. M., & Pavlyuk, N. N. 2015, *Information Bulletin on Variable Stars*, 6140, 1
- Van Dyk, S. D., Zheng, W., Brink, T. G., et al. 2018, *ApJ*, 860, 90
- Wang, L. J., Wang, X. F., Cano, Z., et al. 2019, *MNRAS*, 489, 1110
- Whitesides, L., Lunnan, R., Kasliwal, M. M., et al. 2017, *ApJ*, 851, 107
- Wilkinson, D. M., Maraston, C., Goddard, D., Thomas, D., & Parikh, T. 2017, *MNRAS*, 472, 4297
- Xiang, D., Wang, X., Mo, J., et al. 2019, *ApJ*, 871, 176
- Yokoo, T., Arimoto, J., Matsumoto, K., Takahashi, A., & Sadakane, K. 1994, *PASJ*, 46, L191
- Zhang, K., Wang, X., Zhang, J., et al. 2016, *ApJ*, 820, 67
- Zhang, T., Wang, X., Wu, C., et al. 2012, *AJ*, 144, 131